Icarus 328 (2019) 127–140

Contents lists available at ScienceDirect

Icarus

journal homepage: www.elsevier.com/locate/icarus

Comparative study between rivers in Tarim Basin in northwest China and Evros Vallis on Mars

Sheng Gou[a,b], Zongyu Yue[a], Kaichang Di[a,b,*], Yi Xu[b]

[a] State Key Laboratory of Remote Sensing Science, Institute of Remote Sensing and Digital Earth, Chinese Academy of Sciences, Beijing 100101, China
[b] State Key Laboratory of Lunar and Planetary Sciences, Macau University of Science and Technology, Macau 999078, China

ARTICLE INFO

Keywords:
Tarim Basin
Evros Vallis
Morphometric parameters
Quantitative comparison
Formation mechanism

ABSTRACT

The morphometric characteristics of the Kaidu River and Keriya River in the extremely arid Tarim Basin, and the Evros Vallis on Mars were compared to study the formation of the dendritic Evros Vallis, which has great significance for exploring ancient climate of Mars. The following results were obtained: (a) the average sinuosities of Kaidu River, Keriya River, and Evros Vallis are 1.17, 1.35, and 1.32 respectively. (b) the average bifurcation ratios are 3.84, 4.73 and 3.43 respectively. (c) the average stream length ratios are 2.21, 3.86 and 2.08 respectively. (d) the stream frequencies are 0.017, 0.028 and 0.002 respectively. (e) the drainage densities are 0.195 km^{-1} and 0.217 km^{-1}, and 0.048 km^{-1} respectively. (f) the stream gradients are 3.74‰, 7.03‰ and 1.63‰ respectively. (g) the stream fractal dimensions are 1.70, 1.0 and 1.68 respectively. Paleodischarge estimations at different stream segments of Evros Vallis support the hypothesis that the V-bend area that joints the eastern and western segments possibly has a tectonic origin. Geomorphological evidence (e.g., tributaries) from high-resolution images and stream morphometric parameters from a comparative analysis (e.g., concave upward longitudinal profile and stream fractal dimension) support previous hypothesis that Evros Vallis is a mature drainage system formed by precipitation-driven surface runoff. This drainage process occurred either in a continuously warm-wet climate that lasted long enough on early Mars or in regional hydrologic cycles consisting of precipitation and occasionally returned runoff in intermittently clement climates.

1. Introduction

The discovery of fluvial valleys on Mars from Mariner 9 images (Masursky, 1973) has greatly triggered scientists' interest and raised further discussions on the possibility of the emergence of life on the planet. The widespread valley networks, fluvial deltas and alluvial fans observed on today's Martian surface are the best evidence of past sustaining water-related erosion and deposition activities (Howard et al., 2005; Baker, 2006; McSween, 2006; Hynek et al., 2010). These geomorphologies indicate a completely different climatic condition in the past, possibly warmer and wetter than present cold and dry environment (Fairen, 2010; Hynek et al., 2010; Wade et al., 2017).

With the high-resolution images collected from recent Mars missions, including Mars Global Surveyor, Mars Odyssey, Mars Express, and Mars Reconnaissance Orbiter, the distribution of Martian valley networks has been studied in detail. Most of the Martian valley systems formed around the Noachian-Hesperian boundary (~3.8–3.6 Ga), while others continued through the Hesperian and into the Early Amazonian (~2.8 Ga) (Hynek et al., 2010). Quantitative measures of stream profiles and basin shapes show that most Martian drainage basins are less developed than terrestrial counterparts (Stepinski and Coradetti, 2004). There are many proposed formation mechanisms for the valley networks on Mars, which have important implications on Martian paleoclimate, that are still under debate, e.g., precipitation, basal melting of snow, groundwater sapping, ground-ice melting, episodic flooding, paleolake outflows, debris flows (Nummedal and Prior, 1981; Robinson and Tanaka, 1990; Malin and Carr, 1999; Craddock and Howard, 2002; Luo, 2002; Carr and Head, 2003; Montgomery and Gillespie, 2005; Hoke and Hynek, 2009).

The present Martian surface atmospheric pressure varies from around 0.03 kPa to over 1.155 kPa, with a mean surface level pressure of 0.60 kPa. The Martian surface temperature varies from lows of about −140 °C during the polar winters, to highs of up to 20 °C in summers (Bolonkin, 2009). Thus, today's Martian surface is generally frozen and uninhabitable. However, the observed water-related geomorphologies (e.g., valley networks, paleolakes, and deltaic deposits) tell a different story about Mars' past. On Earth, insufficient recharge forms intermittent or ephemeral rivers, while continuous water supply leads to

* Corresponding author at: No. 20A, Datun Road, Chaoyang District, Beijing 100101, China.
E-mail address: dikc@radi.ac.cn (K. Di).

https://doi.org/10.1016/j.icarus.2019.03.017
Received 6 July 2018; Received in revised form 19 November 2018; Accepted 13 March 2019
Available online 21 March 2019
0019-1035/

perennial rivers, each of these has distinguished hydrological and morphometric characteristics and play important roles in global water cycling. Studies on Martian topography, global distribution of deltas and valleys proposed the northern lowland was possibly occupied by an ancient ocean, which covered up to one-third of the planet's surface (Head et al., 1999; Di Achille and Hynek, 2010; Luo et al., 2017). This hypothesis explains why the most highly dissected regions are located between the equator and mid-southern latitudes (Luo and Stepinski, 2009).

Located south of the large Schiaparelli impact basin in the southern highlands, the Evros Vallis is an ancient valley that has a dendritic drainage pattern. The dendritic pattern is the most common type throughout nature, it forms in regions where the underlying rock structure does not strongly control the position of stream channels and develops in areas where the rocks have roughly equal resistance to weathering and erosion, for example, sandstone and shale (Gabler et al., 2008). The formation of the dendritic Evros Vallis is still under debate, which can be categorized into three main hypotheses. (1) **Discharge of localized water source.** Because no similar networks are found in the surrounding terrain, Gulick (1996) proposed that the isolated valley system of the Evros Vallis was unlikely formed as a result of widespread rainfall, but a localized water source, such as discharge of a hydrothermal system or localized melting of snowfall, seems more consistent. (2) **Ephemeral discharges or immature drainage system.** Som et al. (2009) studied the width-area, slope-area and distance-area relationships for 10 largest valley systems with various ages (only the eastern section of the Evros Vallis was studied). They found these scaling parameters do not satisfy the terrestrial empirical values, hence, they suggested Martian dendritic networks were formed in either an arid to semiarid climate with infrequent and local precipitation events that triggered ephemeral discharges or a very short period of warm-wet climate that produces immature drainage systems. (3) **Long and stable fluvial runoff.** Howard et al. (2005) studied the geomorphological features of 4 channel systems (including Evros Vallis) in the Martian highlands, they held that these channels were formed by fluvial processes during the latest Noachian or early to mid-Hesperian. Hoke and Hynek (2009) mapped, crater age-dated, and analyzed geomorphology, stream order, and drainage density for the 10 largest valley networks (including the entire Evros Vallis), they found morphologies and drainage densities that suggest those valleys formed primarily by precipitation (surface runoff erosion). Caprarelli and Wang (2012) found the concave longitudinal profile of Evros Vallis is consistent with that of a mature valley, produced by long and stable runoff caused by sustained precipitation in the Martian ancient past. Considering the vast difference between these hypotheses, it is important to implement analog studies, which may help reach a consensus regarding the formation mechanism for the dendritic Evros Vallis.

As one of China's inland basins, the Tarim basin in northwest China hosts a great number of distinct geomorphologies that are particularly like those observed on today's Martian surface. These features include sand dunes with different morphologies, yardangs with streamlined protuberances, playas with layered deposits, polygons with variable sizes and shapes, gullies of different scales, and valley networks with flood/alluvial plains. These typical aeolian and fluvial landforms, together with the large temperature fluctuations between day and night, as well as present-day extreme arid climate, make the Tarim Basin another potential terrestrial analog site in China for Mars research, in addition to the Qaidam basin (Xiao et al., 2017). Kaidu River and Keriya River are located in the north and south of the Tarim Basin respectively. Both have dendritic drainage patterns, which are very similar to the dendritic Evros Vallis observed from orbital images. However, the water supply, which is an important factor for the formation of a drainage system, of these two rivers is different. The Kaidu River is primarily recharged by mixed water from snowmelt and rain (Xu et al., 2008), while the Keriya River is chiefly dependent on glacier/snow meltwater (Chen, 1988). The geomorphologies and topographies of these two drainage systems are not affected by human activities (e.g., artificial channels), and most of the stream channels of Keriya River lack rooted vegetation. Hence, they are appropriate examples of arid environments for a comparative study to explore the possible aqueous past and arid present environments of Mars.

Researchers have used the morphometry of Martian valleys to determine processes responsible for valley network formation. For example, Ansan and Mangold (2006) quantitatively analyzed morphology and morphometry of Warrego Valles (bifurcation ratio, length ratio, area ratio, etc.), which are consistent with a terrestrial fluvial valley network. Their study supports the assertion that valley networks formed by fluvial processes are controlled by the atmospheric water cycle. Luo and Stepinski (2009) inferred precipitation-fed runoff erosion in a warm and wet early Mars as the primary mechanism of valley formation from relatively high drainage density derived from topographic data. Stepinski et al. (2004) and Stepinski and Stepinski (2005) analyzed drainage networks on Earth and Mars using fractal and morphology analysis and concluded that an arid terrestrial environment (e.g., Atacama Desert) provides the best terrestrial morphologic analog for Martian valley network sites. These pioneering studies have evaluated the applicability of well-established relations of terrestrial fluvial morphology to those on Martian valley networks. This study focuses on the comparative analysis of morphometric characteristics between the Evros Vallis on Mars and the Kaidu River and Keriya River in the Tarim Basin and aims to test the previously stated hypotheses to understand the formation of the Evros Vallis.

2. Regional and geological settings

2.1. Kaidu River and Keriya River in Tarim Basin

The Tarim basin, located in the south of Xinjiang Uyghur Autonomous Region of China, is bordered by several mountain ranges, the Kunlun Mountains to the southwest, the Tibet Plateau to the southeast, the Pamir Mountains to the west, and the Tian Shan Mountains to the north (Fig. 1). Because it is far from the ocean and the surrounding mountains block most of the moisture sources to the region, the Tarim basin is characterized by extremely arid conditions (Jin et al., 1994). The average annual precipitation is only 116.8 mm, but the average annual evaporation is as high as 2500–3400 mm, resulting in much of the basin being occupied by the Taklamakan Desert, which is the driest region of Eurasia with an annual precipitation in its center of < 20 mm (Jin et al., 1994). As one of the largest endorheic drainage basins in the world, the Tarim River mainly consists of 114 rivers from 9 drainage systems in radial centripetal planform that surrounds the Tarim Basin (Liu et al., 2006). The Kaidu River and Keriya River, whose branching and dendritic organizations are very similar to dendritic Evros Vallis observed on Mars from orbital images, are selected as terrestrial analogs for fluvial morphometry comparisons in this study.

The Kaidu River drainage basin is situated in the north-east of Tarim Basin (Fig. 1). The terrain of the basin is higher on the north and west than on south and east, with an average elevation of 3100 m (Fig. 2). The Kaidu River originates from the central part of the Tian Shan Mountains and ends in the Bosten Lake. It's primarily recharged by mixed water from snowmelt and rain (Xu et al., 2008). The drainage basin above Da Shan Kou hydrological station, with a catchment area of about 1.8×10^4 km^2, is chosen as the study area in this paper.

The Keriya River drainage basin is located in the south of Tarim Basin (Fig. 1). The Keriya River is a seasonal river that originates from the Kunlun Mountains and flows northward (Fig. 3). 71% of the river's water supply is heavily dependent on glacier/snow meltwater, 20% comes from groundwater seepage, and only 9% directly from local precipitation (Chen, 1988). Because of intense evapotranspiration, the downstream of the river vanishes into the sand dunes of the Taklamakan desert in the center of the Tarim Basin (Yang, 2001; Yang et al., 2002). Because most of the stream channels lack rooted vegetation and

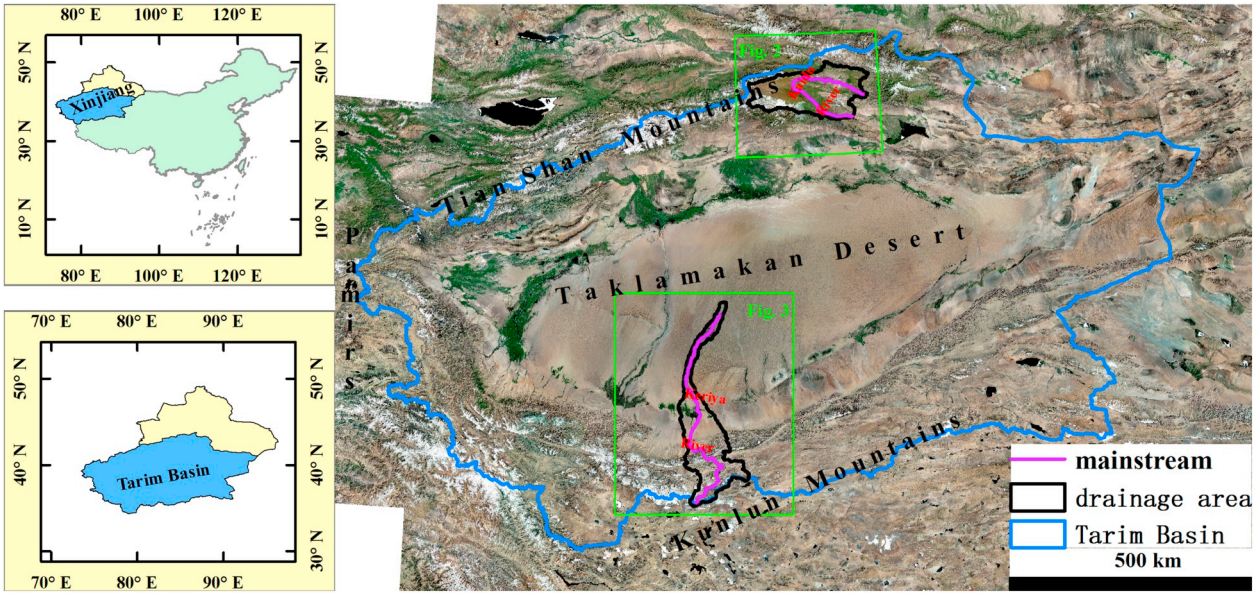

Fig. 1. Location of Kaidu River and Keriya River within Tarim Basin. The upper left inset marks the location of Xinjiang in China, the lower left inset indicates the location of Tarim Basin in Xinjiang, and the right inset marks the location of Kaidu River, Keriya River, and Taklamakan Desert within Tarim Basin and the surrounding mountains. The green boxes denote the extents of Fig. 2 and Fig. 3. (For interpretation of the references to color in this figure legend, the reader is referred to the web version of this article.)

the human activities (e.g., artificial channels) are restricted to limited oases, the Keriya River drainage basin, which retains its original topography and geomorphology, is an ideal terrestrial analog for a comparative study.

2.2. Evros Vallis on Martian surface

Straddling the Martian dichotomy boundary and flowing from east to west, the ~ 800 km dendritic Evros Vallis is located between the Meridiani Planum and the Noachis Terra. The elevation in this drainage basin ranges from approximately −1900 to 3800 m (Fig. 4). The middle Noachian highland (mNh) unit occurs almost entirely in the Evros Vallis, except for early Noachian highland (eNh) unit covers a small portion of the drainage basin in the northeast. Heavily cratered landscape and subsequent geological activities are clearly visible in this region, for example, gullies on the crater walls, sand ripples on the bottom of the Evros Vallis.

Desiccation mud cracks and rampart craters are observed within the channel of Evros Vallis (Fig. 5). Desiccation mud cracks are formed only at the sediment-air interface (Plummer and Gostin, 1981), and rampart craters are evidence of liquid water or ice on the subsurface of Mars (Carr et al., 1977). The distinctive well-preserved ejecta blanket (Fig. 5) of the rampart crater indicates that it was formed later, after the channel was active. These widespread geomorphological evidences strongly suggest water existed on the surface of Mars in the past, and the valley networks of Evros Vallis were carved by runoff. Based on the above observations, the morphometric parameters of Evros Vallis are computed and compared with those of the Kaidu River and Keriya River in the following sections.

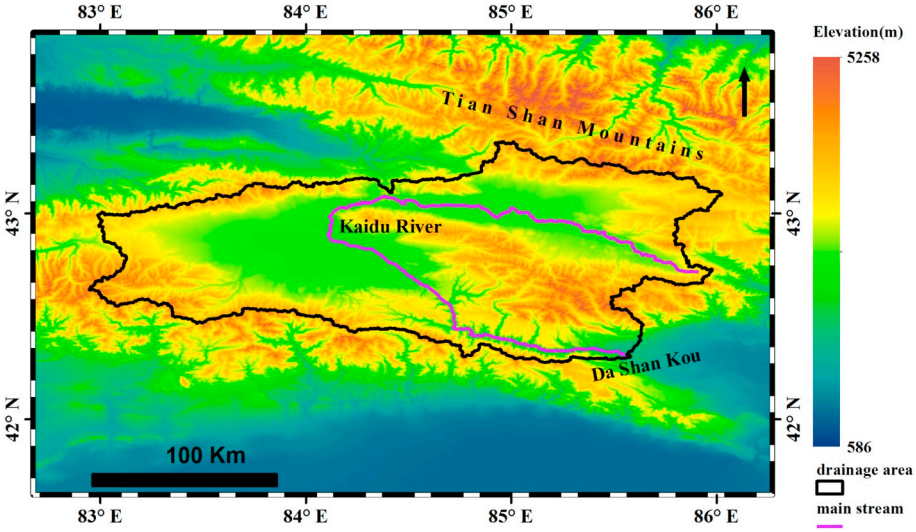

Fig. 2. ASTER DEM of Kaidu River drainage basin.

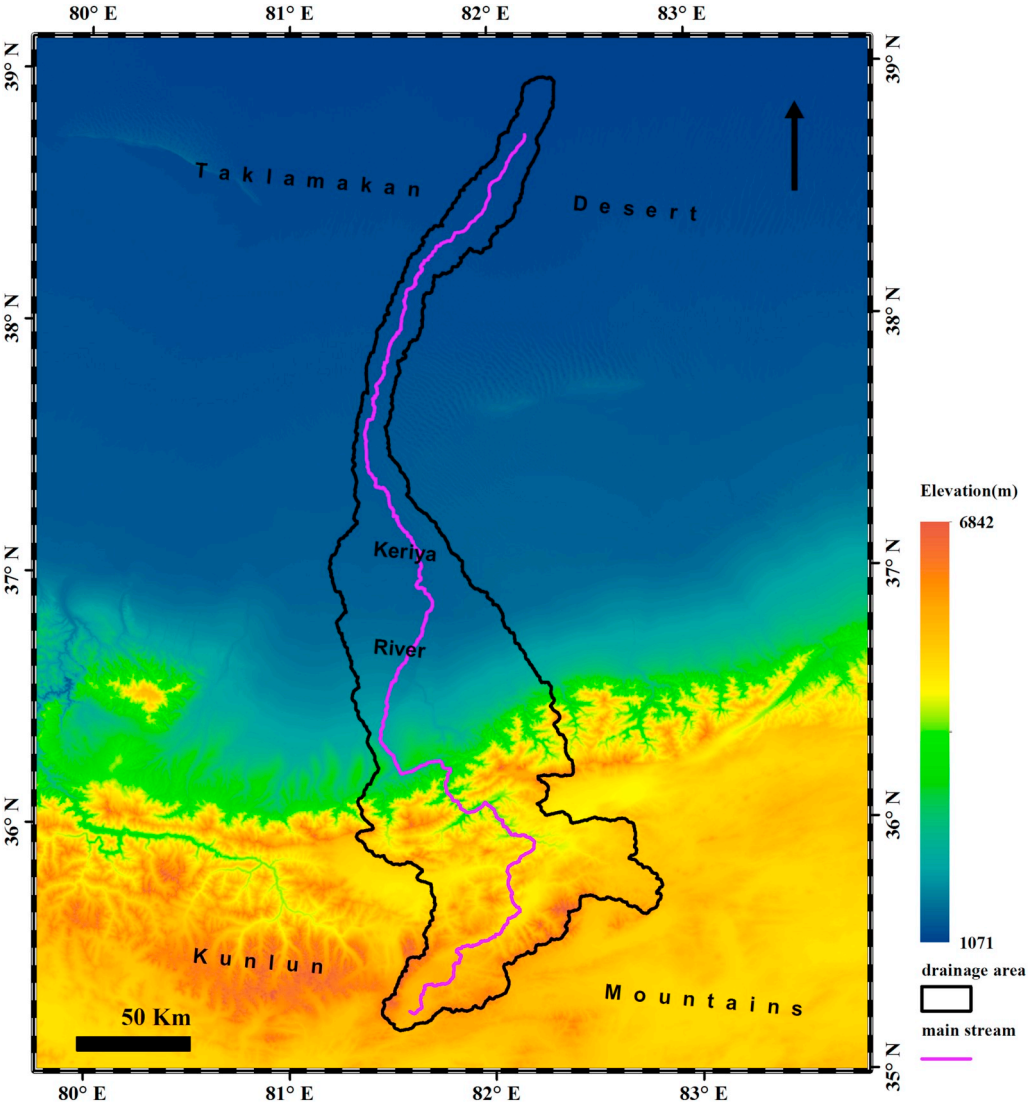

Fig. 3. ASTER DEM of Keriya River drainage basin.

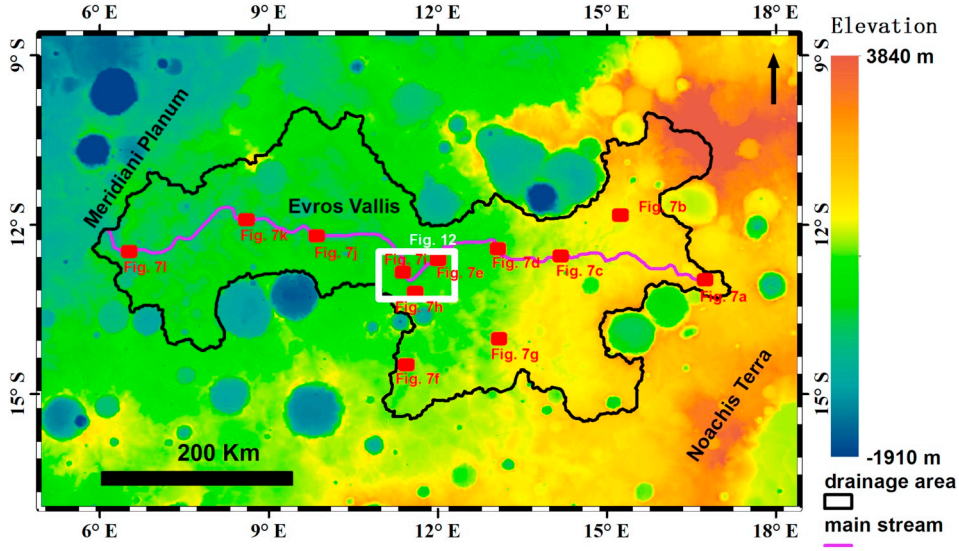

Fig. 4. MOLA elevation of Evros Vallis drainage basin (the red and white rectangles frame the areas shown in detail in Fig. 7 and Fig. 12). (For interpretation of the references to color in this figure legend, the reader is referred to the web version of this article.)

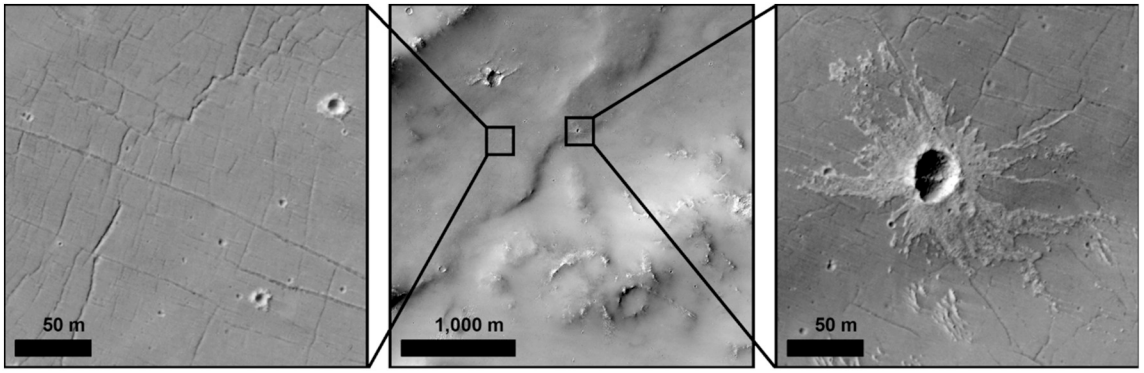

Fig. 5. Desiccation mud cracks and rampart crater observed within the Evros Vallis (HiRISE image ID: ESP_018661_1680_RED). North is up.

3. Data sources

3.1. Terrestrial datasets

3.1.1. ASTER GDEM

The Advanced Spaceborne Thermal Emission and Reflection Radiometer (ASTER) Global Digital Elevation Model (GDEM), covering land surfaces between 83°N and 83°S, was jointly developed and distributed by METI of Japan and NASA of United States (Tachikawa et al., 2011a). The GDEM version 2 released in 2011 is the public available elevation data with higher resolution and accuracy than its previous version. It has a spatial resolution of about 30 m, with horizontal and vertical accuracy of about 82 m and 17 m respectively (Tachikawa et al., 2011b).

3.1.2. GaoFen-1 images

GaoFen-1 is the first satellite of a series of China's high-resolution earth observation satellites, which operates on sun-synchronous orbit with nominal altitudes of about 645 km. There are six push-broom cameras on GaoFen-1 satellite, including two panchromatic/multispectral (PMS) cameras and four wide-field-of-view (WFV) cameras. The PMS cameras, have jointly a swath about 60 km wide (2 × 30 km), observe in four spectral bands (Blue: 445–520 nm, Green: 520–590 nm, Red: 630–690 nm, and Infrared: 770–890 nm) and one panchromatic band (450–900 nm), with a resolution of about 8 m and 2 m for multispectral and panchromatic images, respectively. The WFV cameras also observe in four spectral bands with a resolution of about 16 m and a joint wide coverage reach up to about 800 km (4 × 200 km) (Bai, 2013).

3.2. Martian datasets

3.2.1. CTX images

The Context Camera (CTX) is a facility instrument onboard Mars Reconnaissance Orbiter (MRO), which provides grayscale context images (500–800 nm) with a pixel resolution up to about 6 m that span 30 km across from MRO's near-circular, near-polar mapping orbit of about 290 km altitude. CTX makes observations simultaneously with the high-resolution images from the High-Resolution Imaging Science Experiment (HiRISE) and the hyperspectral images from the Compact Reconnaissance Imaging Spectrometer for Mars (CRISM), providing a broader context for the data collected by the other two instruments. In addition, CTX observes features of interest to NASA's Mars Exploration Program (e.g., candidate landing sites), and conducts a scientific investigation of geologic, geomorphic, and meteorological processes on Mars (Malin et al., 2007).

3.2.2. HiRISE images

The High-Resolution Imaging Science Experiment (HiRISE) is a scientific instrument onboard MRO, with a spatial resolution of up to about 30 cm from a 255 × 320 km orbit. HiRISE COLOR and RED images are acquired via 14 CCD detectors at identical photometric angles, with multiple choices for pixel binning and number of time delay and integration lines. The COLOR image has a swath width of 1.2 km consisting of three-color bands (RED: 570–830 nm, blue-green (BG): 400 to 600 nm, near infrared (NIR): 800–1000 nm), and the RED image has a single band with 6 km wide swath. These high-resolution images provide unprecedented views of layered materials, gullies, channels, and other science targets, in addition to characterizing possible future landing sites. (McEwen et al., 2007).

3.2.3. Other datasets

In addition, Martian global products also are used in this research. These products are mainly collected from the scientific community on the USGS Astrogeology's PIGWAD website (https://webgis.wr.usgs.gov/). These datasets include: (1) global distribution of Martian valley networks in vector format provided by Hynek et al. (2010); (2) the Mars Odyssey (MO) Thermal Emission Imaging System (THEMIS) daytime infrared (IR) mosaic image with a resolution of about 100 m/pixel (Edwards et al., 2011).

4. Method

4.1. Stream network delineation for Keriya River and Kaidu River

The resolution of ASTER elevation is about 30 m/pixel. However, Mars Orbiter Laser Altimeter (MOLA) elevation (Smith et al., 2001) is the only available global elevation for Mars and it has a resolution of about 500 m/pixel. The large resolution difference between them may cause scale issues, for example, MOLA elevation is too coarse to resolve many small features. THEMIS daytime IR mosaic image with a resolution of about 100 m/pixel, which reduces resolution difference greatly, have already been used to manually map Martian valley networks (Hynek et al., 2010). Thus, MOLA elevation was not used in this study. The digitized Evros Vallis by Hynek et al. (2010) is cited for further calculation directly in this study.

The stream networks of Kaidu River and Keriya River are delineated from ASTER elevation by following the algorithm shown in Fig. 6. All the raster analysis steps in the algorithm were implemented in the Arc Hydro and Hydrology toolbox of the ArcGIS software.

Step 1. **DEM reconditioning.** The mainstreams networks polylines of Kaidu and Keriya River were firstly burned into the raw DEM with the AGREE method (Hellweger, 1997) by the Arc Hydro's DEM Reconditioning Tool in order to increase the degree of agreement between stream networks delineated from the DEM and the input vector stream networks. DEM-reconditioned raster was derived in this step.

Fig. 6. Flow chart of delineating stream networks from the ASTER DEM.

Step 2. **Fill sinks.** Because of data resolution or noise issues, there were terrain construction artifacts in the elevation. The filling sinks step modified the AGREE-reconditioned DEM to eliminate the unreal non-physical sinks and ensure the water can smoothly flow in the elevation grid. DEM-filled raster was derived.

Step 3. **Determine flow direction.** The surface flow direction in each elevation pixel of the sink-filled DEM was then assigned based on the steepest downward slope (O'Callaghan and Mark, 1984; Fairfield and Leymarie, 1991). Flow direction raster was thus derived.

Step 4. **Calculate flow accumulation.** The flow accumulation in each elevation pixel is then calculated, which is a measure of the drainage area that records the total number of pixels draining through a given pixel. Pixels with higher flow accumulation values are located in areas of lower elevation, such as in valleys or drainage channels.

Step 5. **Define streams.** The catchment area threshold T for defining streams is of key importance because it controls the meaningfulness or representativeness of existing streams. Drainage density decreases rapidly when threshold increases at first, however, it becomes stable and tends to be flat when the drainage density is consistent with real situation. Instead of applying the default threshold, 1% of the maximum flow accumulation in the Stream Definition Tool, the threshold in this study is determined by using the algorithm proposed by Kong and Li (2005). The relationship between drainage density and threshold is fitted by a power function F(T) and the inflection point of the power function (solve T for $F''(T) = 0$) was considered as a rational threshold in this study. The stream definition raster was then visually compared and checked with the elevation data.

Step 6. **Segment and vectorize streams.** The flow direction raster and stream definition raster were used as inputs for the Stream Segmentation Tool to divide the stream into segments and each segment was coded with a unique id number. The segmentation raster was then converted into polyline with the Drainage Line Processing Tool.

Step 7. **Assign and vectorize stream orders.** The Strahler (1952) stream order for each stream was assigned by the Stream Order Tool, and the stream order raster was also converted into polyline.

Step 8. **Delineate and vectorize sub-basins.** The sub-basin for each stream segment was delineated with the Catchment Grid Delineation Tool and converted into polygon with the Catchment Polygon Processing Tool.

The smallest resolvable valid valley segment for this proposed algorithm is limited by the elevation data resolution (about 6 pixels), which is about 30 m/pixel for ASTER DEM. Thus, any stream network of < 180 m cannot be delineated by ArcGIS in this study. After the above semi-automatic processing steps, the stream networks and sub-basins in Kaidu River and Keriya River Basin were delineated and vectorized for further analysis.

4.2. Calculation of morphometric parameters

The development of a drainage system over space and time is influenced by several variables such as geology, structural components, geomorphology, soil and vegetation of an area through which it flows (Magesh et al., 2013). Thus, values of morphometric parameters are extremely important for detailed statistical, analytical, and comparative analysis of drainage basins. Both fundamental morphometric parameters and derived sophisticated parameters that summarize the characteristics of the drainage basin are calculated for the Kaidu River and Keriya River in the Tarim Basin and the Evros Vallis on Mars, including drainage area, stream length, stream order, stream number, stream frequency, drainage density, mean stream length, stream sinuosity, bifurcation ratio, length ratio, stream slope, and fractal dimension (Horton, 1945; Strahler, 1957; La Barbera and Rosso, 1989). The definitions and implications of these parameters are stated below, with the equations listed in Table 1.

(a) Drainage area is a basic parameter that refers to the entire area drained by a stream or a system of connecting streams such that all streamflow originating in the area is discharged through a single outlet (Linsley et al., 1949).

(b) Stream length is the distance measured along the flow direction from the stream source to the outlet. It is indicative of chronological

Table 1
Formula and definition of morphometric parameters of drainage basin.

Parameters	Formula/Definition	References
drainage area (*A*)	area of the drainage basin	(Horton, 1945)
stream length (*L*)	length of the stream from source in the watershed to the outlet.	(Horton, 1945)
stream number (*N*)	number of stream segments	(Horton, 1945)
stream order (*u*)	stream hierarchical order	(Horton, 1945)
stream frequency (*Fs*)	$Fs = N/A$, N is the total number of all the stream segments and A is the area of the drainage basin	(Horton, 1945)
drainage density (*Dd*)	Dd = *Ltotal/A*, *Ltotal* is the total length of all the stream segments and *A* is the area of the drainage basin	(Horton, 1945)
mean stream length (*Lm*)	*Lm = Lu/Nu*, Lu is the total stream length of the order u and Nu is the number of stream segments of the order u	(Horton, 1945)
stream sinuosity (*Ssinu*)	*Ssinu = Ls/Lv*, *Ls* is the length of the actual stream and *Lv* is the length of straight-line distance.	(Horton, 1945)
stream length ratio (*RL*)	*RL = Lu/Lu-1*, Lu is the total length of the order u and Lu-1 is the total stream length of the next lower order u-1	(Horton, 1945)
bifurcation ratio (*Rb*)	*Rb = Nu/Nu + 1*, Nu is the number of stream segments of the order u and *Nu + 1* is the number of stream segments of the next higher order *u + 1*	(Horton, 1945)
stream gradient (slope)	*Sslope = Edif/Ddif*, Edif is the elevation difference between pour and head/source of the stream, *Ddif* is the distance between pour and head/source	(Horton, 1945)
fractal dimension (*D*)	*D* = max[1, *logRb/logRL*], *Rb* is the mean bifurcation ratio and *RL* is the mean stream length ratio.	(La Barbera and Rosso, 1989)

developments of the stream segments and surface runoff characteristics (Magesh et al., 2013). Streams with relatively shorter lengths are representative of areas with steep slopes and fine textures, whereas longer stream lengths are generally indicative of low gradients (Strahler, 1964).

(c) Stream order is a measure of the position of a stream in the hierarchy of tributaries (Leopold et al., 1964). Strahler stream ordering (Strahler, 1957) is one widely applied schema for stream classification and is adopted in this study.

(d) Stream number is the number of streams of different orders in the drainage basin, which generally decreases gradually as the stream order increases (Magesh et al., 2013). The occurrence of stream segments depends on the nature and structure of rocks, vegetation cover, nature and amount of rainfall and soil permeability (Magesh et al., 2013).

(e) Stream frequency is the ratio of the total number of streams of all orders in the basin to the total area of the basin (Horton, 1945). It is more or less dependent on the rainfall and the physiography of the region and is an index of the various stages of landscape evolution (Magesh et al., 2013).

(f) Drainage density is defined as the ratio of total stream length in a given basin to the total drainage area (Horton, 1945). It indicates the closeness of stream channels and the degree of drainage development, thus determines the water travel time and provides a numerical measurement of landscape dissection and runoff potential (Chorley, 1969).

(g) Mean stream length is calculated by dividing the total stream length of a given order by the number of streams in that order. It is a characteristic property related to the drainage and its associated surfaces (Strahler, 1964).

(h) Stream sinuosity is calculated by dividing the length of the stream segment by the straight line distance between the endpoints of the stream (Mueller, 1968). It reflects the channel bank resistance to lateral erosion and the percentage of silt/clay in channel bank sediment (Ebisemiju, 1994), which is higher in meandering gravel or sand bedded streams and lower in confined mountain streams.

(i) Bifurcation ratio, defined as the ratio of the number of stream segments of given order to the number of segments of the next higher order, is an index of relief and dissections, (Horton, 1945). It is highly stable and shows a small range of variation for different regions or environments, except where powerful geologic controls dominate (Strahler, 1957).

(j) Stream length ratio, defined as the ratio of the mean stream length of one order to the next lower order of the stream segments. It has an important relationship with surface flow and discharge (Horton, 1945).

(k) Stream gradient (slope), usually expressed as meters per kilometer, is the ratio of drop in elevation between two points of a stream and the distance between them, in which the water actually flows. The flow velocity, and thus stream power is directly related to the stream slope, the steeper the slope, the faster the velocity of flow. Changes in the gradient along a stream generally correspond to differences in bedrock or introduced load (Hack, 1973).

(l) Fractal dimension quantifies the irregularity or complexity of an individual stream or a stream network (Schuller et al., 2001). It is used to investigate the scaling properties of the attributes and parameters describing drainage basin form and process (La Barbera and Rosso, 1989).

The basic parameters, such as drainage area, stream length, and stream number, vary greatly among different drainage basins. However, the derived parameters, especially the dimensionless ones, such as stream sinuosity, length ratio, and bifurcation ratio, have either theoretically predicted or robust terrestrial empirical values across different bedrock geology and topography that can be used for comparisons and analyses and thus provide a statistical basis for judgment of similarity or difference.

4.3. Paleodischarge estimation for the Evros Vallis

Paleodischarge is an indicator for analyzing ancient climate and fluvial erosion on Mars. The empirical correlative form-discharge relationship (Osterkamp and Hedman, 1982) between terrestrial channel form (most commonly channel width (W, m)) and discharge (Q, m^3/s) have been extensively used after scaled for the putative effect of gravity (Irwin et al., 2005; Jaumann et al., 2005; Williams and Weitz, 2014). However, recent analyses on submarine channels and rivers show reduced-gravity environment lowers the driving force and forms shallower channel slopes, and thus the application of a scaling relationship for differences in gravity is unnecessary (Konsoer et al., 2013).

Jacobsen and Burr (2016) confirmed causal width-discharge relationship (Eq. (1)) derived from hydraulic geometry is more accurate and precise for estimating discharge for a Martian-terrestrial analog river than the correlative width-discharge correlation derived from Missouri River Basin. The hydraulic geometry data for deriving the causal width-discharge relationship are bankfull widths and bankfull discharges from four continents, which comprise a wide range of median grain sizes (< 0.062 mm to > 25 mm), terrestrial environments, and bank strengths. Thus, hydraulic geometry relationship, which is more consistent with in-situ and modeling estimate, provides alternative for estimating paleodischarge on Mars.

Martian valleys are always heavily infilled with aeolian, volcanic and impact materials, which obscure the evidence of fluvial bedforms. Thus, Martian valleys that contain obvious identifiable inner channels are extremely rare, whereas valleys with no clearly defined inner channels are much more common (Som et al., 2009). Since modifications such as mass wasting, impact gardening, aeolian infilling and lava flow mantling have not greatly altered the original Martian valley shape after fluvial activity ceased, many Martian valleys have obvious valley boundaries (Williams and Phillips, 2001). Hence, valley width becomes a plausible substitute for bankfull width in the hydraulic geometry relationship (Eq. (1)) for estimating fluvial paleodischarge of Evros Vallis in this study.

$$Q = 0.08W^{1.908} \quad (1)$$

The valley width is measured at different locations along the upstream, midstream and downstream of Evros Vallis on CTX images (Fig. 7). The width of each stream segment is measured at least three times, and the final width values for paleodischarge estimation are averages of all measurements made within each stream segment, which can reduce the measuring error.

5. Results and discussions

5.1. Stream networks and morphometric parameters

5.1.1. Morphometry of the Kaidu River

The stream network delineation result of the Kaidu River is shown in Fig. 8. There are 253 stream segments of the five stream orders within the 18,348.47 km^2 Kaidu River drainage basin delineated in this study (Fig. 8). The total length of all the streams is 3581.46 km, so the drainage density is 0.195 km^{-1} and the stream frequency is 0.014. Other morphometric parameters of the Kaidu River are shown in Table 2. The average stream sinuosity is 1.35 and the stream fractal dimension is 1.70.

5.1.2. Morphometry of the Keriya River

The stream network delineation result of the Keriya River is shown in Fig. 9. There are 561 stream segments of the five stream orders within the 19,977.30 km^2 Keriya River drainage basin delineated in this study (Fig. 9). The total length of all the streams is 4340.74 km, so the drainage density is 0.22 km^{-1} and the stream frequency is 0.028. Other

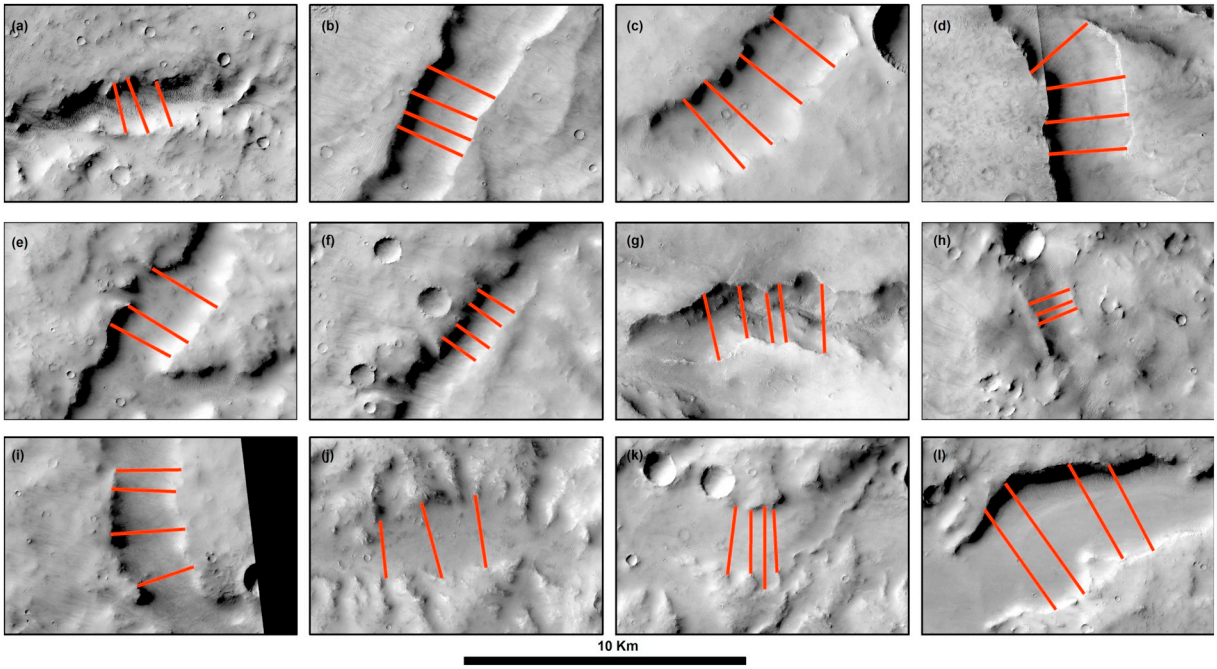

Fig. 7. CTX images with different stream segments for measuring valley width (red lines). Their locations are marked in Fig. 4 by the white box. North is up. (CTX image IDs from a to l: B19_017052_1685_XN_11S343W, B20_017474_1684_XN_11S344W, J03_046102_1651_XI_14S345W, P07_003695_1663_XI_13S346W, B21_017751_1695_XI_10S348W, G22_026810_1652_XN_14S348W, G13_023131_1649_XI_15S347W, B20_017606_1662_XN_13S348W, B20_017250_1694_XI_10S349W, B12_014349_1673_XN_12S350W, G01_018806_1696_XI_10S351W and B20_017593_1685_XI_11S353W). (For interpretation of the references to color in this figure legend, the reader is referred to the web version of this article.)

morphometric parameters of the Keriya River are shown in Table 3. The average stream sinuosity is 1.32 and the stream fractal dimension is 1.0.

5.1.3. Morphometry of the Evros Vallis

There are 548 stream segments of the six stream orders within the 8949.54 km^2 Evros Vallis with a total length of 8949.54 km (Fig. 10), so the drainage density is 0.08 km^{-1} and the stream frequency is 0.005. The other morphometric parameters of the Evros Vallis are shown in Table 4. The average stream sinuosity is 1.17 and the calculated stream fractal dimension is 1.68.

5.2. Comparison of the morphometric parameters

The morphometric parameters of these drainage basins are discussed in detail in the following sub-sections.

5.2.1. Average stream length and sinuosity

Table 2, Table 3 and Table 4 show that the average length of the first order stream (the smallest tributary) of the Evros Vallis is much larger than that of the Kaidu River and Keriya River, which is consistent with Irwin et al. (2008) who discovered that Martian drainage basins tend to be more elongated.

Stream sinuosity is closely related to the channel bedrock, channel gradient, dominant particle size and other factors (Rosgen, 1994). The

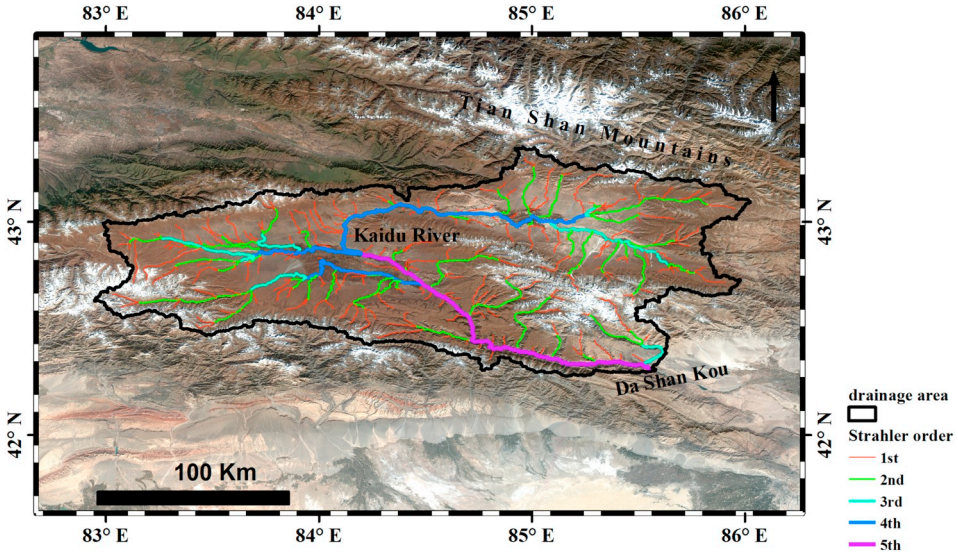

Fig. 8. Streams of Kaidu River overlaid on GF-1 image.

Table 2
Morphometric parameters of the Kaidu River.

Stream order	Stream number	Total stream length(km)	Mean stream length(km)	Average stream sinuosity	Bifurcation ratio	Length ratio
1	196	1935.08	9.87	1.24	4.45	–
2	44	976.57	22.19	1.26	4.89	2.25
3	9	227.15	25.24	1.35	3.00	1.14
4	3	281.05	93.68	1.40	3.00	3.71
5	1	161.61	161.61	1.49	–	1.73

average sinuosities of all stream segments of Kaidu River, Keriya River, and Evros Vallis are 1.35, 1.32 and 1.17 respectively, showing the former two rivers have relatively more twists and turns, and the latter is straighter.

5.2.2. Average bifurcation and length ratio

Horton (1945) considered the bifurcation ratio as a representation of relief. It is usually constant for all orders of streams in a reasonably homogeneous basin and it characteristically ranges between 3.0 and 5.0. Strahler (1957) further demonstrated the bifurcation ratio is highly stable and shows a small range of variation for different regions/environments except where powerful geological controls dominate. The mean bifurcation ratios for the Kaidu River, Keriya River, and the Evros Vallis are 3.84, 4.73 and 3.43 respectively. This indicates the drainage pattern of the three basins hasn't been affected by the geologic structural disturbances.

Observations on natural networks without unusual geological controls indicate that the stream length ratio is usually between 1.5 and 3.5 (Smart, 1972). The average stream length ratios for Kaidu River, Keriya River, and Evros Vallis are 2.21, 3.86 and 2.08 respectively. The untypical mean stream length ratio value of the Keriya River results from the unusual surface runoff characteristics. The tributaries develop well in the upstream (Fig. 9), and the small mean length of the 1st order stream (4.54 km in Table 3) reflects large slope and fine texture in the river source area. However, the recharge in the downstream of the Keriya River drainage basin is extremely scanty, and the terminal of the river is lost in the drifting sand dunes of the Taklamakan desert. Hence the stream length ratio between the 5th order and the 4th order is

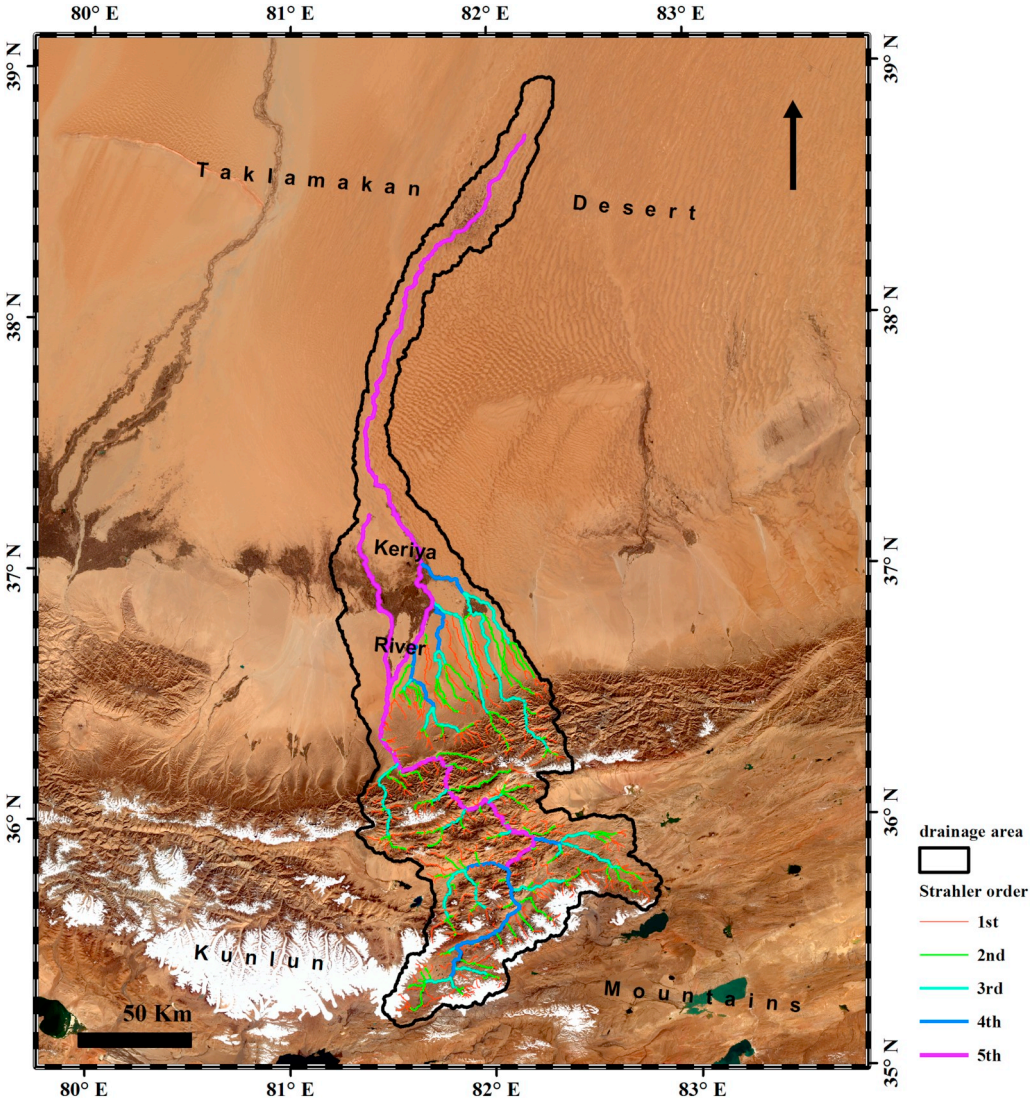

Fig. 9. Streams of Keriya River overlaid on GF-1 image.

Table 3
Morphometric parameters of the Keriya River.

Stream order	Stream number	Total stream length(km)	Mean stream length(km)	Average stream sinuosity	Bifurcation ratio	Length ratio
1	426	1933.88	4.54	1.22	4.10	–
2	104	1019.13	9.80	1.24	4.52	2.16
3	23	567.69	24.68	1.29	3.29	2.52
4	7	220.74	31.53	1.32	7.00	1.28
5	2	599.31	299.65	1.53	–	9.50

extremely high (9.5), which causes the average ratio value of all orders of streams to become unusual.

5.2.3. Drainage density and stream frequency

The drainage densities on Mars range from 0 over large areas of volcanic plains to 0.3–0.5 km^{-1} locally on some volcanoes (Carr and Chuang, 1997), and the terrestrial values are in the range of 1–100 km^{-1}, which vary chiefly with the precipitation rate and subsequent redistribution of water (Abrahams, 1984). The drainage density of the Kaidu River and the Keriya River are 0.195 km^{-1} and 0.217 km^{-1} respectively (Table 5). They are far less than the typical terrestrial values, indicating the extremely arid climate conditions in the Tarim Basin greatly confine the development of drainage network. The drainage density of the Evros Vallis is only 0.048 km^{-1} (Table 5), roughly 4 orders of magnitude less than comparably acquired terrestrial values, indicating the low terrestrial drainage density values in extremely arid local drainage basins are still much larger than that on Mars. The stream frequencies for Kaidu River, Keriya River, and Evros Vallis are 0.017, 0.028 and 0.002 respectively.

5.2.4. Mainstream gradient and fractal dimension

The mainstream gradients of the Kaidu River, Keriya River, and the Evros Vallis are 3.74‰, 7.03‰ and 1.63‰ respectively (Table 5). According to Rosgen Stream Classification System (Rosgen, 1994), the channels can be divided into four types by their gradient (Table 6), thus, all of them can be regarded as low gradient streams.

The longitudinal profile of the Kaidu River (Fig. 11a) can be split into two sections; the section from source to about 200 km is concave upward with a slope of 2.54‰ and the other section from 200 km to the outlet is concave downward with a slope of 5.18‰. The longitudinal profile of the Keriya River (Fig. 11b) also features two sections, the first one, from the source to 330 km is an approximate 12.21‰ steep straight channel, and the other section from 330 km to the vanishing terminal in the desert is an almost flat channel with a slope of 0.89‰. Although the infilling effects of the main channel cannot be excluded completely, the general trend of the whole longitudinal profile of the Evros Vallis (Fig. 11c) is gently concave upward.

The stream fractal dimensions of the Kaidu River, Keriya River. and the Evros Vallis are 1.70, 1.0 and 1.68 respectively.

5.3. Paleodischarge of the Evros Vallis

Table 7 lists the estimated paleodischarge of different segments of the Evros Vallis. The general trend illustrates the estimated paleodischarge increases gradually from the upstream to the downstream. For example, the estimated paleodischarges for the upstream tributaries at Fig. 7a and Fig. 7b are about 1.4×10^5 m^3/s and 2.6×10^5 m^3/s respectively, while for the downstream estuary shown in Fig. 7l is about 6.3×10^5 m^3/s. This value is the same order of magnitude as derived by Hoke et al. (2011) when estimating paleodischarge with flow depth of 40 m. It indicates that the dendritic tributaries and confluences effectively add more discharge to the mainstream.

Note that though the stream in Fig. 7i is the confluence of the streams in Fig. 7e and Fig. 7h (Fig. 12), the estimated paleodischarge in Fig. 7i is even less than that in Fig. 7e. Caprarelli and Wang (2012) thought the approximately 90° angle of the sharp V-shape bend (indicated by the black arrow in Fig. 12), as well as the linear extent of the incisions in the west and east of the bend, is related with tectonic origin. If this scenario is true, it indicates that tectonic activities may have changed the physical properties of local underlying substrates that leads the water loss increases around the V-bend area. And it also means that the tectonic activities happened ahead or at least simultaneously with the surface runoff.

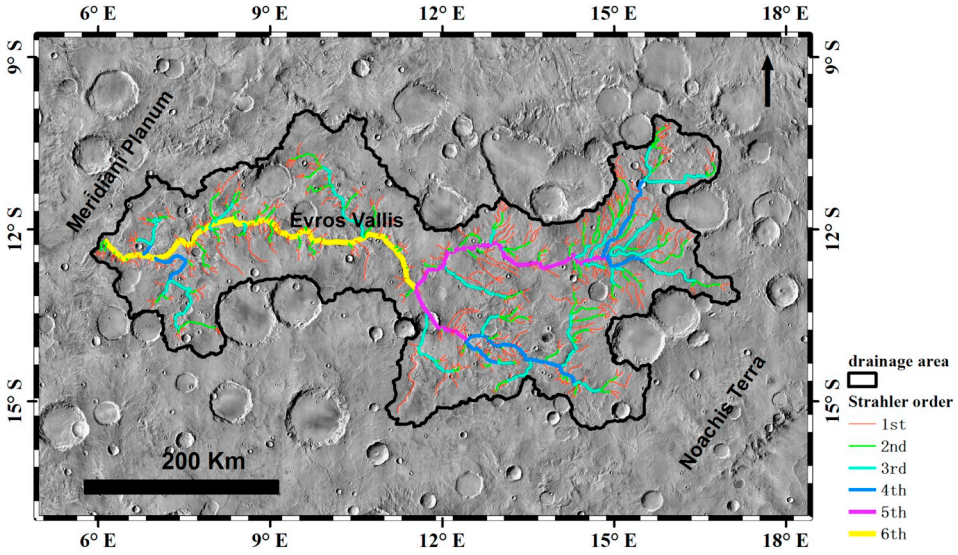

Fig. 10. Streams of Evros Vallis (Hynek et al., 2010) overlaid on THEMIS daytime infrared mosaic.

Table 4
Morphometric parameters of the Evros Vallis.

Stream order	Stream number	Total stream length(km)	Mean stream length(km)	Average stream sinuosity	Bifurcation ratio	Length ratio
1	396	4771.18	12.05	1.07	3.63	–
2	109	1885.29	17.30	1.07	3.30	1.44
3	33	1133.57	34.35	1.14	4.71	1.99
4	7	414.56	59.22	1.28	3.50	1.72
5	2	336.60	168.30	1.18	2.00	2.84
6	1	408.34	408.34	1.26	–	2.43

Table 5
Morphometric parameters of the drainage basins.

Drainage	Total length (km)	Total stream number (#)	Drainage area (km2)	Drainage density (km-1)	Stream frequency (#/km2)	stream slope (‰)	Stream fractal dimension
Kaidu River	3581.46	314	18,348.47	0.195	0.017	3.74	1.70
Keriya River	4340.74	561	19,977.30	0.217	0.028	7.03	1.00
Evros Vallis	5039.78	163	105,905.72	0.048	0.002	1.63	1.68

Table 6
Classification of channels by gradient (Rosgen, 1994).

Channel type	Slope
very steep channel	> 0.10
steep channel	0.04–0.10
moderate gradient channel	0.02–0.04
low gradient channel	< 0.02

5.4. Discussions for the formation of Evros Vallis

Subsurface ice gradually depletes between ± 30° (Fanale et al., 1986), and the ground ice is not stable in equatorial region (0° ~ 30°) (Mellon and Jakosky, 1995; Mellon et al., 2004). The Evros Vallis drains westward from 20°E to 5°E at about 12°S. Only two hydrous mineral outcrops have been detected so far in this region (Carter et al., 2013), hence, the hypothesis of discharge of localized water source (Gulick, 1996) is less likely to be the scenario for the formation of the Evros Vallis drainage system.

After analyzing a large sample of field data, La Barbera and Rosso (1989) found typical stream fractal dimension of river networks to lie between 1.5 and 2, with an average of 1.6–1.7. He and Zhao (1996) further partitioned it to describe the geomorphologic evolution stage of the drainage basin. When the stream fractal dimension lies between 1.0 and 1.6, it indicates the stream networks of the drainage basin is in its young stage, between 1.6 and 1.89 indicates a mature stage, and between 1.89 and 2.0 indicates an old stage. The value of this parameter for Keriya River (1.0) indicates the stream network is not yet well developed, which suggests that the Keriya River is still young, this is consistent with inference from the relative high stream slope. The stream fractal dimension of Evros Vallis (1.68) shows a mature drainage system. In addition, the concavity of the stream longitudinal profile reflects its evolutionary stage. The older the river is, the more concave its longitudinal profile becomes (Radoane et al., 2003). The gently concave-up longitudinal profile of Evros Vallis (Fig. 11c) shows its mature development. Stream morphometric parameters from the comparative analysis (e.g., concave upward longitudinal profile and stream fractal dimension) support previous studies that Evros Vallis is a mature drainage system, hence, the hypothesis of ephemeral discharges or immature drainage system (Som et al., 2009) can also be excluded.

Desiccation mud cracks and rampart craters observed in the channel of Evros Vallis (Fig. 5) are indicators of past flow activity. Theoretically, high gradient streams tend to have steep, narrow V-shaped valleys and are referred to as young streams. Low gradient streams have wider and less rugged valleys, with a tendency for the stream to meander (Sarp and Duzgun, 2015). Since the mainstream gradient of Evros Vallis (1.63‰) is much less than those of the Kaidu River (3.74‰) and Keriya River (7.03‰), its sinuosity should be higher. However, the comparison shows the average sinuosity of Evros Vallis (1.17) is less than those of the Kaidu River (1.35) and Keriya River (1.32). The contradiction may be caused by later aeolian, cratering, and mass wasting processes that infilled the Martian valley and changed the elevation difference. Hence, it is inappropriate here to relate the transversal profiles of the streams with slope and sinuosity.

Though recharge mainly from glacier/snowpack meltwater can form dendritic drainage system (the upstream of the Kaidu River and Keriya River shown here as terrestrial analog), the drainage pattern cannot remain dendritic without enough recharge (the downstream of Keriya River in this study). The drainage pattern of the entire Evros Vallis is dendritic with obvious tributaries flowing toward the mainstream, indicating a sustained water supply. However, the location of Evros Vallis (12°S, 12°E) was unlikely to be covered by ice during Mars high-obliquity periods (Karlsson et al., 2015; Dundas et al., 2018), implying that the water source cannot be mainly from melting, but from other sources.

The atmospheric pressure and the temperature on the present-day Martian surface are significantly less than what is needed to sustain liquid water. However, geomorphological and geochemical features also suggest that Mars was wet and relatively warm during the mid to late Noachian (Jakosky and Phillips, 2001; Solomon et al., 2005), and several theories/models have been proposed to explain warm and wet climate once existed on the early Mars (Phillips et al., 2001; Segura et al., 2008; Feng et al., 2009). Seybold et al. (2018) found the geometries of valley networks on Mars most resembled those found among terrestrial arid landscapes, and they support valley networks were formed primarily by flow erosion, which requires frequent precipitation and an active hydrological cycle. Hence, the dendritic morphology and geomorphological evidence from high-resolution orbital images (e.g., tributaries), like terrestrial networks recharged mainly by rainfall, suggests that precipitation-driven surface runoff, rather than other water sources (e.g., groundwater sapping), is responsible for the formation of Evros Vallis. This means either a period of continuously warm-wet climate on early Mars lasted long enough for the networks to be carved or regional hydrologic cycles consisting of precipitation and runoff occasionally returned in intermittently clement climates. Hoke and Hynek (2009) suggested this period have lasted about 210 +/− 50 Ma that straddling the late Noachian and early Hesperian.

6. Conclusion

The Kaidu River and Keriya River in the extremely arid Tarim Basin were chosen as terrestrial analogs for the study of the Evros Vallis in

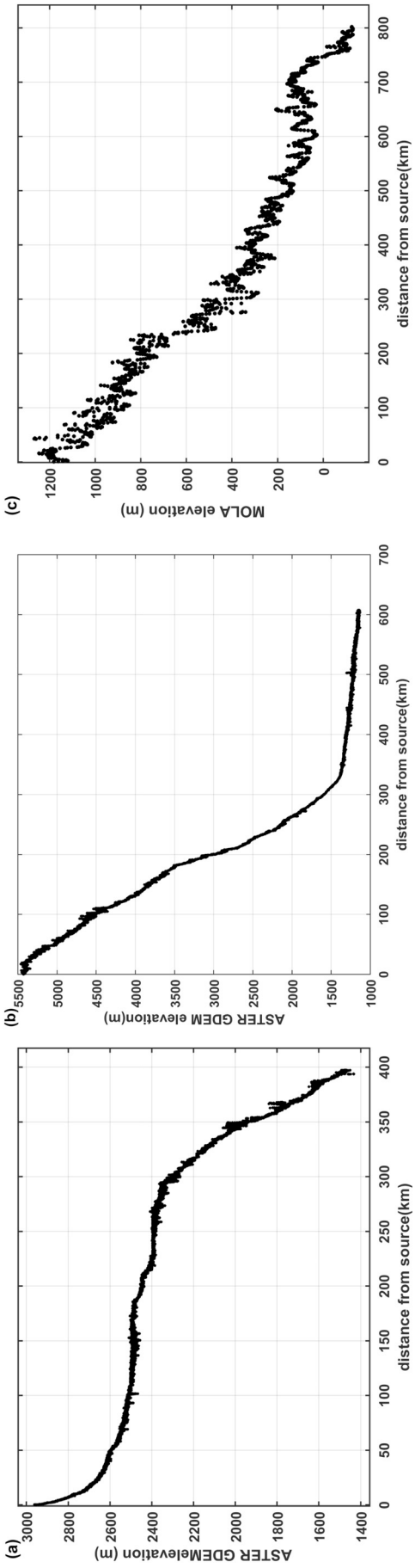

Fig. 11. Longitudinal profile of the main channel: (a) Kaidu River; (b) Keriya River; (c) Evros Vallis. The noises in the profiles are due to the quality of the elevation data.

Table 7
Estimated paleodischarge for different stream segments of the Evros Vallis.

Location	Average bank-full channel width (m)	Estimated paleodischarge (m^3/s)
Fig. 7a	1884	141,954
Fig. 7b	2597	261,672
Fig. 7c	3080	362,383
Fig. 7d	2835	309,393
Fig. 7e	2550	252,822
Fig. 7f	1465	87,841
Fig. 7g	2135	180,138
Fig. 7h	1501	91,946
Fig. 7i	2348	216,017
Fig. 7j	2534	249,718
Fig. 7k	2396	224,466
Fig. 7l	4121	631,571

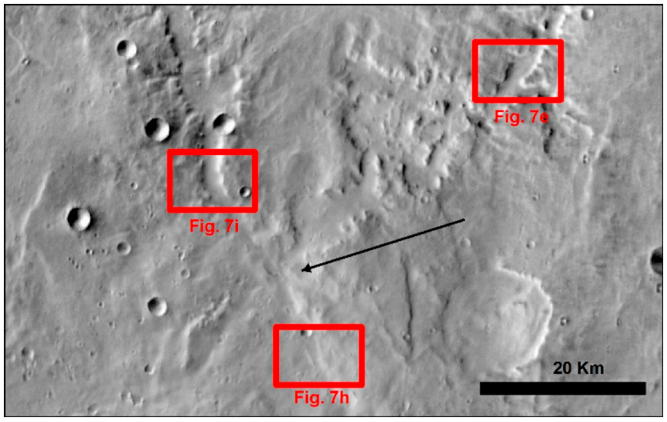

Fig. 12. THEMIS daytime infrared mosaic shows details of the V-bend channel of the Evros Vallis. The black arrow marks the location of the V-bend. North is up.

Mars. Their stream networks were firstly delineated from ASTER elevation with semi-automatic processing algorithms. Morphometric parameters of the dendritic drainage basins for Evros Vallis on Mars, Kaidu River, and Keriya River were then quantitatively calculated and compared. The main comparison results and implications are: (1) The average length of the smallest tributary of Evros Vallis is much larger than those of the Kaidu River and Keriya River, and their average sinuosities are 1.35, 1.32 and 1.17 respectively, which means the latter two rivers have relatively more twists and turns, while the former is straighter. (2) The mean bifurcation ratios of Kaidu River, Keriya River, and Evros Vallis are 3.84, 4.73 and 3.43 respectively, all of which are within typical value ranges. The average stream length ratios are 2.21, 3.86 and 2.08 respectively, the unusually high value in the Keriya River is due to the insufficient recharge in the downstream that causes the 5th order stream segment becomes extremely long. (3) The drainage densities of Kaidu River, Keriya River, and Evros Vallis are 0.195 km^{-1}, 0.217 km^{-1}, and 0.048 km^{-1} respectively. Though the former two are far less than the typical terrestrial values (1–100 km^{-1}), they are still much larger than that on Mars. The stream frequencies are 0.017, 0.028 and 0.002 respectively. (4) The stream gradients are 3.74‰, 7.03‰ and 1.63‰ respectively and the stream fractal dimensions are 1.70, 1.0 and 1.68 respectively. The concave upward longitudinal profile and fractal dimension value indicate both Kaidu River and Evros Vallis are mature drainage systems, while Keriya River is an immature system.

Paleodischarge is estimated for different stream segments of Evros Vallis. The general trend illustrates the estimated paleodischarge increases gradually from the upstream to the downstream, indicating that the dendritic tributaries and confluences effectively add more discharge to the mainstream. Possible tectonic activities may have changed the

properties of underlying local substrates that led to an increase in water loss around the V-bend area which joints the east and west segments. The tectonic activities may have happened previously or at least simultaneously to the surface runoff.

Three previously proposed hypotheses for the formation of the Evros Vallis were evaluated. Geomorphological evidence from high-resolution images (e.g., tributaries) and stream morphometric parameters from comparative analysis (e.g., concave upward longitudinal profile and stream fractal dimension) support the fact that Evros Vallis is a mature drainage system formed by precipitation-driven surface runoff, which happened either in continuously warm-wet climate that lasted long enough on early Mars or in a regional hydrologic cycles consisting of precipitation and runoff occasionally returned in intermittently clement climates.

Acknowledgments

The research is supported by National Natural Science Foundation of China (grant Nos. 41702354 and 41472303), opening fund of State Key Laboratory of Lunar and Planetary Sciences (Macau University of Science and Technology) (Macau FDCT grant No. 119/2017/A3), Science and Technology Development Fund of Macau (Macau FDCT grant No. 131/2017/A3) and youth talent project of State Key Laboratory of Remote Sensing Science (grant No. 16RC-07). We appreciate the constructive reviews by Prof. James Head and an anonymous reviewer that greatly helped improve the manuscript.

References

Abrahams, A.D., 1984. Channel networks: a geomorphological perspective. Water Resour. Res. 20 (2), 161–188.
Ansan, V., Mangold, N., 2006. New observations of Warrego Valles, Mars: evidence for precipitation and surface runoff. Planetary and Space Science 54 (3), 219–242.
Bai, Z.G., 2013. Technical characteristics of GF-1 satellite. Aerospace China 8, 5–9.
Baker, V.R., 2006. Geomorphological evidence for water on Mars. Elements 2 (3), 139–143.
Bolonkin, A.A., 2009. Artificial environments on Mars. In: Badescu, V. (Ed.), Mars: Prospective Energy and Material Resources. Springer Berlin Heidelberg, Berlin, Heidelberg, pp. 599–625.
Caprarelli, G., Wang, B., 2012. Wet Mars implications of revised scaling calculations for Evros Vallis. Aust. J. Earth Sci. 59 (2), 263–276.
Carr, M.H., Chuang, F.C., 1997. Martian drainage densities. J. Geophys. Res. 102 (E4), 9145–9152.
Carr, M.H., Head, J.W., 2003. Basal melting of snow on early Mars: a possible origin of some valley networks. Geophys. Res. Lett. 30 (24).
Carr, M., Crumpler, L., Cutts, J., Greeley, R., Guest, J., Masursky, H., 1977. Martian impact craters and emplacement of ejecta by surface flow. J. Geophys. Res. 82 (28), 4055–4065.
Carter, J., Poulet, F., Bibring, J.P., Mangold, N., Murchie, S., 2013. Hydrous minerals on Mars as seen by the CRISM and OMEGA imaging spectrometers: updated global view. J. Geophys. Res. 118, 1–28.
Chen, H.S., 1988. Effect of water in eco-geographic environment of the keriya river valley. J. Desert Res. 8 (2), 38–53.
Chorley, R.J., 1969. Introduction to Physical Hydrology. Methuen and Co. Ltd., Suffolk.
Craddock, R.A., Howard, A.D., 2002. The case for rainfall on a warm, wet early Mars. J. Geophys. Res. 107, 21–1-21-36.
Di Achille, G., Hynek, B.M., 2010. Ancient Ocean on Mars supported by global distribution of deltas and valleys. Nat. Geosci. 3 (7), 459–463.
Dundas, C. M.,et al., 2018. Exposed subsurface ice sheets in the Martian mid-latitudes. Science. 359(6372), 199–201.
Ebisemiju, F.S., 1994. The sinuosity of alluvial river channels in the seasonally wet tropical environment: case study of river elemi, southwestern Nigeria. CATENA 21 (1), 13–25.
Edwards, C., Nowicki, K., Christensen, P., Hill, J., Gorelick, N., Murray, K., 2011. Mosaicking of global planetary image datasets: 1. Techniques and data processing for thermal emission imaging system (THEMIS) multi-spectral data. J. Geophys. Res. 116 (E10), E10008.
Fairen, A.G., 2010. A cold and wet Mars. Icarus 208 (1), 165–175.
Fairfield, J., Leymarie, P., 1991. Drainage networks from grid digital elevation models. Water Resour. Res. 27 (5), 709–717.
Fanale, F.P., Salvail, J.R., Zent, A.P., Postawko, S.E., 1986. Global distribution and migration of subsurface ice on Mars. Icarus 67 (1), 1–18.
Feng, T., K., J.F., S., S.C., 2009. Thermal escape of carbon from the early Martian atmosphere. Geophys. Res. Lett. 36 (2).
Gabler, R.E., Petersen, J.F., Trapasso, L.M., Sack, D., 2008. Physical Geography. Brooks Cole, USA.
Gulick, V.C., 1996. Hydrogeological interpretation of candidate origin sites for Martian meteorite ALH84001. In: 28th Annual Meeting of Division for Planetary Sciences. Bulletin of the American Astronomical Society, Tucson, AZ; United States, pp. 1059.
Hack, J.T., 1973. Stream-profile analysis and stream-gradient index. Journal of Research of the U.S. Geological Survey. 1 (4), 421–429.
He, L.H., Zhao, H., 1996. The fractal dimension of river networks and its interpretation. Sci. Geogr. Sin. 16, 124–128.
Head, J.W., Hiesinger, H., Ivanov, M.A., Kreslavsky, M.A., Pratt, S.F., Thomson, B.J., 1999. Possible ancient oceans on Mars: evidence from Mars orbiter laser altimeter data. Science 286 (5447), 2134–2137.
Hellweger, F., 1997. AGREE-DEM surface reconditioning system. http://www.ce.utexas.edu/prof/maidment/GISHYDRO/ferdi/research/agree/agree.html.
Hoke, M.R., Hynek, B.M., 2009. Roaming zones of precipitation on ancient Mars as recorded in valley networks. J. Geophys. Res. 114 (E8), E08002.
Hoke, M.R., Hynek, B.M., Tucker, G.E., 2011. Formation timescales of large Martian valley networks. Earth Planet. Sci. Lett. 312 (1), 1–12.
Horton, R.E., 1945. Erosional development of streams and their drainage basins; hydrophysical approach to quantitative morphology. Geol. Soc. Am. Bull. 56 (3), 275–370.
Howard, A.D., Moore, J.M., Irwin, R.P., 2005. An intense terminal epoch of widespread fluvial activity on early Mars: 1. Valley network incision and associated deposits. J. Geophys. Res. 110 (E12), E12S14.
Hynek, B.M., Beach, M., Hoke, M.R.T., 2010. Updated global map of Martian valley networks and implications for climate and hydrologic processes. J. Geophys. Res. 115 (E9), E09008.
Irwin, R.P., Craddock, R.A., Howard, A.D., 2005. Interior channels in Martian valley networks: discharge and runoff production. Geology 33 (6), 489–492.
Irwin, R.P.I., Howard, A.D., Craddock, R.A., 2008. In: Rice, S.P., Roy, A.G., Rhoads, B.L. (Eds.), Fluvial valley networks on Mars. Wiley, Chichester, UK, pp. 419–451.
Jacobsen, R.E., Burr, D.M., 2016. Greater contrast in Martian hydrological history from more accurate estimates of paleodischarge. Geophys. Res. Lett. 43 (17), 8903–8911.
Jakosky, B.M., Phillips, R.J., 2001. Mars' volatile and climate history. Nature 412, 237.
Jaumann, R.,et al., 2005. Interior channels in Martian valleys: constraints on fluvial erosion by measurements of the Mars express high resolution stereo camera. Geophys. Res. Lett. 32(16).
Jin, J., Dong, G.R., Shen, J.Y., 1994. The contemporary climate of Tarim Basin, XinJiang. Journal of Arid Land Resources and Environment 8, 12–21.
Karlsson, N.B., Schmidt, L.S., Hvidberg, C.S., 2015. Volume of Martian midlatitude glaciers from radar observations and ice flow modeling. Geophys. Res. Lett. 42 (8), 2627–2633.
Kong, F.Z., Li, L.L., 2005. Determination of drainage area threshold for extracting valley netwroks by digital elevation model. Water Resour. Power 23, 65–67.
Konsoer, K., Zinger, J., Parker, G., 2013. Bankfull hydraulic geometry of submarine channels created by turbidity currents: relations between bankfull channel characteristics and formative flow discharge. Journal of Geophysical Research: Earth Surface 118 (1), 216–228.
La Barbera, P., Rosso, R., 1989. On the fractal dimension of stream networks. Water Resour. Res. 25 (4), 735–741.
Leopold, L.B., Wolman, M.G., Miller, J.P., 1964. Fluvial Processes in Geomorphology. W. H. Freeman & Company, San Francisco, California.
Linsley, R.K, Kohler, M.A, Paulhus, J.L., 1949. Applied Hydrology. McGraw-Hill, New York.
Liu, S., et al., 2006. Impact of the glacial change on water resources in the Tarim River Basin. Acta Geograph. Sin. 61, 482–490.
Luo, W., 2002. Hypsometric analysis of margaritifer sinus and origin of valley networks. J. Geophys. Res. 107 (1-1-1-10).
Luo, W., Stepinski, T.F., 2009. Computer-generated global map of valley networks on Mars. J. Geophys. Res. 114 (E11), E11010.
Luo, W., Cang, X., Howard, A.D., 2017. New Martian valley network volume estimate consistent with ancient ocean and warm and wet climate. Nat. Commun. 8, 15766.
Magesh, N.S., Jitheshlal, K.V., Chandrasekar, N., Jini, K.V., 2013. Geographical information system-based morphometric analysis of Bharathapuzha river basin, Kerala, India. Appl Water Sci 3 (2), 467–477.
Malin, M.C., et al., 2007. Context camera investigation on board the Mars reconnaissance orbiter. J. Geophys. Res. 112 (E5), E05S04.
Malin, M.C., Carr, M.H., 1999. Groundwater formation of martian valleys. Nature 397 (6720), 589–591.
Masursky, H., 1973. An overview of geological results from Mariner 9. J. Geophys. Res. 78 (20), 4009–4030.
McEwen, A.S., et al., 2007. Mars reconnaissance orbiter's high resolution imaging science experiment (HiRISE). J. Geophys. Res. 112 (E5), E05S02.
McSween, H.Y., 2006. Water on Mars. Elements 2 (3), 135–137.
Mellon, M.T., Jakosky, B.M., 1995. The distribution and behavior of Martian ground ice during past and present epochs. Journal of Geophysical Research: Planets 100 (E6), 11781–11799.
Mellon, M.T., Feldman, W.C., Prettyman, T.H., 2004. The presence and stability of ground ice in the southern hemisphere of Mars. Icarus 169 (2), 324–340.
Montgomery, D.R., Gillespie, A., 2005. Formation of Martian outflow channels by catastrophic dewatering of evaporite deposits. Geology 33 (8), 625–628.
Mueller, J.E., 1968. An introduction to the hydraulic and topographic sinuosity indexes. Ann. Assoc. Am. Geogr. 58 (2), 371–385.
Nummedal, D., Prior, D.B., 1981. Generation of Martian chaos and channels by debris flows. Icarus 45 (1), 77–86.
O'Callaghan, J.F., Mark, D.M., 1984. The extraction of drainage networks from digital elevation data. Computer Vision, Graphics, and Image Processing 28 (3), 323–344.
Osterkamp, W.R., Hedman, E.R., 1982. Perennial-Streamflow Characteristics Related to Channel Geometry and Sediment in Missouri River Basin. (Professional Paper).
Phillips, R. J.,et al., 2001. Ancient geodynamics and global-scale hydrology on Mars.

Science. 291(5513), 2587–2591.
Plummer, P., Gostin, V., 1981. Shrinkage cracks: desiccation or synaeresis? J. Sediment. Res. 51 (4).
Radoane, M., Rădoane, N., Dumitriu, D., 2003. Geomorphological evolution of longitudinal river profiles in the Carpathians. Geomorphology 50 (4), 293–306.
Robinson, M.S., Tanaka, K.L., 1990. Magnitude of a catastrophic flood event at Kasei Valles, Mars. Geology 18 (9), 902–905.
Rosgen, D.L., 1994. A classification of natural rivers. Catena 22 (3), 169–199.
Sarp, G., Duzgun, S., 2015. Morphometric evaluation of the Afşin-Elbistan lignite basin using kernel density estimation and Getis-Ord's statistics of DEM derived indices, SE Turkey. J. Asian Earth Sci. 111, 819–826.
Schuller, D.J., Rao, A.R., Jeong, G.D., 2001. Fractal characteristics of dense stream networks. J. Hydrol. 243 (1), 1–16.
Segura, T.L., Toon, O.B., Colaprete, A., 2008. Modeling the environmental effects of moderate-sized impacts on Mars. Journal of Geophysical Research: Planets 113 (E11).
Seybold, H.J., Kite, E., Kirchner, J.W., 2018. Branching geometry of valley networks on Mars and Earth and its implications for early Martian climate. Sci. Adv. 4 (6).
Smart, J.S., 1972. In: Chow, V.T. (Ed.), Channel networks. Elsevier, pp. 305–346.
Smith, D. E.,et al., 2001. Mars orbiter laser altimeter: experiment summary after the first year of global mapping of Mars. Journal of Geophysical Research: Planets. 106(E10), 23689–23722.
Solomon, S. C.,et al., 2005. New perspectives on ancient Mars. Science. 307(5713), 1214–1220.
Som, S.M., Montgomery, D.R., Greenberg, H.M., 2009. Scaling relations for large Martian valleys. J. Geophys. Res. 114 (E2), E02005.
Stepinski, T., Coradetti, S., 2004. Comparing morphologies of drainage basins on Mars and Earth using integral-geometry and neural maps. Geophys. Res. Lett. 31 (15).
Stepinski, T.F., Stepinski, A.P., 2005. Morphology of drainage basins as an indicator of climate on early Mars. Journal of Geophysical Research: Planets 110 (E12).
Stepinski, T.F., Collier, M.L., Mcgovern, P.J., Clifford, S.M., 2004. Martian geomorphology from fractal analysis of drainage networks. J. Geophys. Res. 109, E02005.
Strahler, A.N., 1952. Hypsometric (area-altitude) analysis of erosional topography. Geol. Soc. Am. Bull. 63 (11), 1117–1142.
Strahler, A.N., 1957. Quantitative analysis of watershed geomorphology. Eos. Transactions American Geophysical Union 38 (6), 913–920.
Strahler, A.N., 1964. Quantitative geomorphology of drainage basins and channel networks. In: Chow, V.T. (Ed.), Handbook of Applied Hydrology. McGraw-Hill, New York, pp. 439–476.
Tachikawa, T., et al., 2011a. ASTER Global Digital Elevation Model Version 2 - Summary of Validation Results. pp. 27.
Tachikawa, T., Hato, M., Kaku, M., Iwasaki, A., 2011b. Characteristics of ASTER GDEM version 2. In: 2011 IEEE International Geoscience and Remote Sensing Symposium, pp. 3657–3660.
Wade, J., Dyck, B., Palin, R.M., Moore, J.D.P., Smye, A.J., 2017. The divergent fates of primitive hydrospheric water on Earth and Mars. Nature 552 (7685), 391–394.
Williams, R.M.E., Phillips, R.J., 2001. Morphometric measurements of martian valley networks from Mars orbiter laser altimeter (MOLA) data. Journal of Geophysical Research: Planets 106 (E10), 23737–23751.
Williams, R.M.E., Weitz, C.M., 2014. Reconstructing the aqueous history within the southwestern Melas basin, Mars: clues from stratigraphic and morphometric analyses of fans. Icarus 242, 19–37.
Yang, X., 2001. The oases along the Keriya River in the Taklamakan Desert, China, and their evolution since the end of the last glaciation. Environ. Geol. 41 (3), 314–320.
Xiao, L., et al., 2017. A new terrestrial analogue site for Mars research: the Qaidam Basin, Tibetan plateau (NW China). Earth Sci. Rev. 164, 84–101.
Xu, J., Chen, Y., Ji, M., Lu, F., 2008. Climate change and its effects on runoff of Kaidu River, Xinjiang, China: a multiple time-scale analysis. Chin. Geogr. Sci. 18 (4), 331–339.
Yang, X., Zhu, Z., Jaekel, D., Owen, L.A., Han, J., 2002. Late quaternary palaeoenvironment change and landscape evolution along the Keriya River, Xinjiang, China: the relationship between high mountain glaciation and landscape evolution in foreland desert regions. Quat. Int. 97-98, 155–166.